Since January 2020 Elsevier has created a COVID-19 resource centre with free information in English and Mandarin on the novel coronavirus COVID-19. The COVID-19 resource centre is hosted on Elsevier Connect, the company's public news and information website.

www.nature.com/gim

Genetics inMedicine

Check for updates

ARTICLE

An integrative multiomics analysis identifies putative causal genes for COVID-19 severity

Lang Wu[1,7]✉, Jingjing Zhu[1,7], Duo Liu[1,2], Yanfa Sun[1,3,4,5] and Chong Wu[6]✉

PURPOSE: It is critical to identify putative causal targets for SARS coronavirus 2, which may guide drug repurposing options to reduce the public health burden of COVID-19.
METHODS: We applied complementary methods and multiphased design to pinpoint the most likely causal genes for COVID-19 severity. First, we applied cross-methylome omnibus (CMO) test and leveraged data from the COVID-19 Host Genetics Initiative (HGI) comparing 9,986 hospitalized COVID-19 patients and 1,877,672 population controls. Second, we evaluated associations using the complementary S-PrediXcan method and leveraging blood and lung tissue gene expression prediction models. Third, we assessed associations of the identified genes with another COVID-19 phenotype, comparing very severe respiratory confirmed COVID versus population controls. Finally, we applied a fine-mapping method, fine-mapping of gene sets (FOGS), to prioritize putative causal genes.
RESULTS: Through analyses of the COVID-19 HGI using complementary CMO and S-PrediXcan methods along with fine-mapping, *XCR1*, *CCR2*, *SACM1L*, *OAS3*, *NSF*, *WNT3*, *NAPSA*, and *IFNAR2* are identified as putative causal genes for COVID-19 severity.
CONCLUSION: We identified eight genes at five genomic loci as putative causal genes for COVID-19 severity.

Genetics in Medicine (2021) 23:2076–2086; https://doi.org/10.1038/s41436-021-01243-5

INTRODUCTION

The coronavirus disease 2019 (COVID-19) pandemic represents a huge public health burden globally. Earlier research has revealed that specific molecular targets are essential for SARS coronavirus 2 (SARS-CoV-2) to enter into human cells [1]. Remdesivir, which blocks such targets, is approved by the US Food and Drug Administration to treat COVID-19. However, currently there remains no effective treatment for COVID-19. Therefore, there is a critical need to uncover additional causal molecular targets for COVID-19. A better characterization of targets can guide drug repurposing for identifying new uses of existing drugs. The fatality rate of COVID-19 is predominantly driven by those patients with severe respiratory failure who are hospitalized [2]. Causal molecular targets that can guide drug repurposing options are thus anticipated to be causally related to COVID-19 severity. However, such causal targets are quite difficult to identify due to the limitations of conventional studies and insufficient biological understanding of human genes.

One strategy to potentially reduce limitations of conventional study designs and identify candidate associated genes is to apply gene-level association tests that aggregate potential regulatory effects of genetic variants on genes [3–7]. Due to the random assortment of genetic alleles transferred from parent to offspring at the time of gamete formation, this approach focusing on genetically predicted gene expression should be less susceptible to selection bias, confounding effects, and reverse causation [8]. In the past several years, we and others have developed novel statistical methods in such transcriptome-wide association studies (TWAS) [3–7, 9]. The conventional TWAS design aims to develop genetic prediction models for gene expression using statistical methods, and further apply the gene expression prediction models to genome-wide association study (GWAS) data sets of the diseases of interest to identify genes with genetically predicted expression and associate them with the diseases. Applying such methods, we and others have conducted TWAS of multiple human diseases and identified multiple disease related genes [3, 5, 8–11].

Besides the conventional TWAS design, there are opportunities to develop novel integrative analyses by incorporating additional epigenetic and functional information. For example, DNA methylation interacts between genome and environment and is established to play an important role in the etiology of multiple diseases. It is known that DNA methylation could potentially regulate expression of genes. In several methylome-wide association studies (MWAS), we found that specific CpG sites could influence disease risk by regulating the expression of disease target genes [12, 13]. In earlier work, we have also shown that integrating information on enhancer–promoter interactions can improve statistical power for gene-level association tests [9, 14]. Built upon these works, we recently developed a novel gene-level association testing method, cross-methylome omnibus (CMO), by integrating genetically regulated DNA methylation in promoters, enhancers, and the gene body to identify disease related genes [15]. As demonstrated in our recent work, through simulation analyses and applied analyses of brain imaging–derived phenotypes and Alzheimer disease, CMO achieves high statistical power while well controlling for the type I error rate [15]. Importantly, CMO could reproducibly identify additional Alzheimer disease–associated genes that are not able to be identified by

[1]Cancer Epidemiology Division, Population Sciences in the Pacific Program, University of Hawaii Cancer Center, University of Hawaii at Manoa, Honolulu, HI, USA. [2]Department of Pharmacy, Harbin Medical University Cancer Hospital, Harbin, China. [3]College of Life Science, Longyan University, Longyan, Fujian, P. R. China. [4]Fujian Provincial Key Laboratory for the Prevention and Control of Animal Infectious Diseases and Biotechnology, Longyan, Fujian, P.R. China. [5]Key Laboratory of Preventive Veterinary Medicine and Biotechnology (Longyan University), Fujian Province University, Longyan, Fujian, P.R. China. [6]Department of Statistics, Florida State University, Tallahassee, FL, USA. [7]These authors contributed equally: Lang Wu, Jingjing Zhu. ✉email: lwu@cc.hawaii.edu; cwu3@fsu.edu

competing methods. This suggests that the novel method of CMO can be a complementary method for TWAS.

Despite the productivity of TWAS design using conventional methods (e.g., TWAS or S-PrediXcan) and novel methods (e.g., CMO) in identifying novel disease-associated genes, it is worth noting that such identified associated genes do not necessarily infer causality [16]. Aligned with other reports, although TWAS is useful for prioritizing causal genes, false positive findings cannot be avoided for some of the identified associations [16]. There are several potential reasons that could induce these, such as correlated expression across individuals, correlated predicted expression, and shared variants [16]. One strategy that can potentially prioritize causal genes in TWAS analyses is fine-mapping. Recently, we and others have developed several methods for fine-mapping in TWAS [17–19]. Focusing on a method we recently developed, fine-mapping of gene sets (FOGS), we find that FOGS adequately controls for type I error rates under various scenarios and performs better than competing methods, including FOCUS and *p* value ranking of TWAS results [17, 19]. Specifically, FOGS could achieve a higher area under the receiver operating characteristic (ROC) curve (AUC), identify more causal genes at the same false positive rate, and yield a smaller number of false positives at the same true positive rate [19].

Herein, we conducted a comprehensive multistage integrative multiomics study leveraging the data from COVID-19 patients and controls included in the COVID-19 Host Genetics Initiative (HGI) [20]. We first applied the CMO method to generate a list of promising genes associated with COVID-19 severity for discovery (comparing 9,986 hospitalized patients versus 1,877,672 population controls). We further applied the conventional S-PrediXcan method to characterize associations of predicted expression of these genes with COVID-19 severity. For associated genes, we further evaluated their associations with another COVID-19 phenotype, comparing very severe respiratory confirmed COVID versus population controls. Finally, we applied the FOGS fine-mapping method to determine the most likely causal genes for severe COVID-19 outcome. In our primary analyses, we focused on blood tissue to capture the systematic pattern of the body. It is also known that the immune system plays an important role in the host response to viral infection. By focusing on blood tissue we can well capture the effects of genes acting in immune related pathways. We also analyzed lung tissue as another likely target tissue for COVID-19 in our S-PrediXcan analyses.

MATERIALS AND METHODS

Genetic association data sets for COVID-19 severity in primary analyses

For evaluation of the association with COVID-19 severity, we used summary statistics data of the most recent version of GWAS analyses from the COVID-19 HGI (Release 5 [January 2021]) [20]. Detailed information on participating studies, quality control, and analyses has been provided on the COVID-19 HGI website (http://www.covid19hg.org/results/). Informed consent was obtained from all subjects. In brief, for discovery analyses comparing hospitalized patients and population controls, data (B2_ALL_eur) from 9,986 hospitalized COVID-19 patients and 1,877,672 population controls from studies in Biobanque Quebec COVID19, Columbia University COVID19 Biobank, Estonian Biobank, Geisinger Health System, Latvia COVID-19 research platform, UCLA Precision Health COVID-19 Biobank, 24Genetics, Amsterdam UMC COVID study group, Determining the Molecular Pathways and Genetic Predisposition of the Acute Inflammatory Process Caused by SARS-CoV-2, COVID19-Host(a)ge, GEN-COVID, reCOVID, deCODE, Million Veterans Program, 23andMe, Bonn Study of COVID19 genetics, FHoGID, Ancestry, The Genetic Predisposition to Severe COVID-19, Genomic, FinnGen, Genetic Modifiers for COVID-19 Related Illness, and UK Biobank were used. Hospitalized COVID-19 cases represented patients with (1) laboratory confirmed SARS-CoV-2 infection (RNA and/or serology based) and (2) hospitalization due to corona-related symptoms. Controls represent those that are not cases. The included subjects are Europeans only, to ensure the homogeneous population structure for the analyses. Only variants with imputation quality > 0.6 were retained. A fixed-effect meta-analysis of individual studies was performed with inverse variance weighting.

CMO test

Details of the CMO method have been described elsewhere [15]. CMO is an integrative gene-level test for identifying associated genes that may impact the trait of interest through DNA methylation pathways. Briefly, three main steps are involved. First, CMO links CpG sites located in enhancers, promoters, and the gene body to a target gene, considering that DNA methylation in enhancers and promoters may also play important roles in gene regulation. Importantly, CMO integrates comprehensive enhancer–promoter interaction information from a comprehensive database called GeneHancer and links CpG sites that are located in the enhancers, promoters, and the gene body to their target genes [21]. Second, by leveraging comprehensive blood DNA methylation genetic prediction models that were developed using a large reference data set involving 4,008 subjects [22], CMO tests associations between genetically regulated DNA methylation of each CpG site and COVID-19 severity using several widely used weighted gene-based tests, including burden, sum of squared score (SSU), and Aggregated Cauchy Association Test (ACAT) tests. The methylation prediction models were developed focusing on 151,729 CpG sites with a significant methylation quantitative trait locus (mQTL), and the lasso method was applied with genetic variants (i.e., single-nucleotide polymoprhisms [SNPs]) closer than 250 kb to each CpG site as potential predictors [22]. Because the optimal test depends on the underlying truth, which is unknown in practice, to maximum statistical power, we apply a Cauchy combination test to combine the results from burden, SSU and ACAT tests [23]. Third, CMO applies a Cauchy combination test to combine statistical evidence from multiple CpG sites for each target gene to determine the associations of target gene–COVID-19 severity. A Benjamini–Hochberg false discovery rate (FDR) of < 0.05 was used to adjust for multiple comparisons.

S-PrediXcan test for candidate genes identified from CMO test

To better characterize the candidate genes identified from the CMO test, we further conducted analyses using the orthogonal and complementary S-PrediXcan method to evaluate associations of their genetically predicted expression with COVID-19 severity [24]. We first leveraged comprehensive blood gene expression genetic prediction models that were developed using a reference data set involving subjects as included in the version 8 of the Genotype-Tissue Expression (GTEx) [25]. A modified cross-tissue UTMOST framework was used to build gene expression genetic models. [26, 27] In brief, SNPs within 1 Mb upstream and downstream of each gene body were included as candidate predictor variables in the model. The residual of the normalized gene expression (TPM) was used for model development after adjustment of age, sex, sequencing platform, the first five principal components (PCs), and probabilistic estimation of expression residuals (PEER) factors. The effect sizes were assessed by minimizing the loss function with a LASSO penalty on the columns (within-tissue effects) and a group LASSO penalty on the rows (cross-tissue effects). The group penalty term implemented sharing of the information from feature (SNP) selection across all the involved tissues. The original model training was modified by unifying the hyperparameter pairs to avoid the overestimation of the prediction performance [26, 27]. The details for the S-PrediXcan method are described elsewhere [24]. Briefly, the associations of genetically predicted gene expression with COVID-19 severity were estimated based on genetic prediction model weights, summary statistics of genetic variants with COVID-19 severity, and a variant correlation (linkage disequilibrium [LD]) matrix. We also tested the associations by leveraging lung tissue gene expression models developed using the same modified UTMOST method [27].

We further evaluated associations of identified genes with another COVID-19 phenotype. Briefly, we compared very severe respiratory confirmed COVID versus population controls by leveraging data sets of A2_ALL_eur (Europeans; 5,101 cases and 1,383,241 controls). S-PrediXcan was used to infer the gene–phenotype associations. We did not compare hospitalized COVID-19 patients versus nonhospitalized COVID-19 patients considering that only a relatively small sample size was available, which may induce insufficient power (B1_ALL_eur data set for Europeans: 4,829 cases and 11,816 controls). We did not investigate the data set of C2_ALL_eur (Europeans; 38,984 cases and 1,644,784 controls), which compared COVID-19 patients versus population controls. This is because

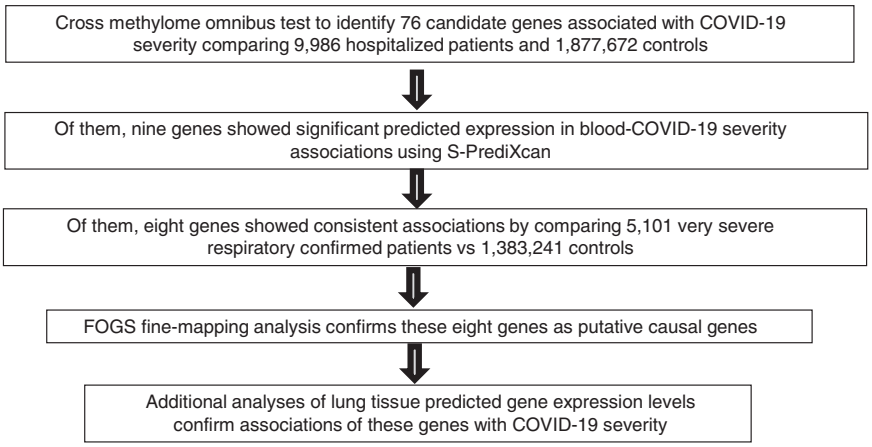

Fig. 1 Study design flow chart. Firstly, we applied cross methylome omnibus (CMO) test and leveraged data from The COVID-19 host genetics initiative (HGI) comparing 9,986 hospitalized COVID-19 patients and 1,877,672 population controls, in which we identified 76 candidate genes. Secondly, we evaluated associations using the complementary S-PrediXcan method and leveraging blood gene expression prediction models, from which nine genes showed an association. Thirdly, we assessed associations of the identified genes with another COVID-19 phenotype, comparing very severe respiratory confirmed COVID vs population controls, and eight of the genes showed consistent associations. We further applied FOGS fine-mapping method which confirms these eight genes as putative causal genes. Finally, additional analyses of lung tissue predicted gene expression confirm associations of these genes with COVID-19 severity.

the outcome of COVID-19 susceptibility would be difficult to interpret, as this may only reflect whether or not an individual was exposed to the SARS-CoV-2 virus.

FOGS fine-mapping analysis to determine putative causal genes for COVID-19 severity

To determine the most likely causal genes for COVID-19 severity, we conducted FOGS fine-mapping analysis for the genes supported by both CMO and S-PrediXcan analyses. Details for FOGS have been described in our earlier publication [19]. In brief, two steps are involved. First, a conditional analysis with ridge regression is conducted to account for the effects of other variants/genes in the locus of interest. Second, FOGS integrates genetic prediction model weights and conditional *Z*-scores by an adaptive test to maintain high statistical power.

RESULTS

The overall study design flow is presented in Fig. 1. The description of several data sets used in this study is included in Supplementary Table 1. Based on the CMO test (Supplementary Table 2; Supplementary Figure 1), we identified significant associations of 76 genes with COVID-19 severity comparing hospitalized patients and population controls at FDR < 0.05 (Table 1). Interestingly, some of these genes tend to be implicated in immunological pathways (Table 1). Of these genes, there were also significant associations between genetically predicted expression in blood tissue of nine genes and COVID-19 severity comparing hospitalized patients and population controls (Table 2). Through analyzing another outcome comparing very severe respiratory confirmed patients versus controls, eight of them (except for *CCR5*) were validated at $P < 0.10$ (Table 2). Based on fine-mapping through FOGS, all these genes at five loci were determined to be putative causal genes. Plots showing associations of SNPs with COVID-19 severity (B2 outcome) at the locus of each of the identified putative causal genes were shown in Supplementary Figures 2–9. Positive associations between predicted expression levels in blood tissue and COVID-19 severity were detected for *XCR1*, *CCR2*, and *OAS3*. Conversely, associations between lower predicted expression levels in blood tissue and increased COVID-19 severity were identified for *SACM1L*, *NSF*, *WNT3*, *NAPSA*, and *IFNAR2*. In analyses of lung tissue gene expression prediction models, although for several of these genes there was no prediction model developed, for the three genes with models available (*CCR2*, *WNT3*, and *IFNAR2*), consistent associations were observed as well (Table 3).

DISCUSSION

This is one of the earliest studies to comprehensively evaluate the associations of genes across the genome with COVID-19 severity using genetic instruments combined with different layers of functional information. After careful assessment including fine-mapping analysis, we identified eight putative causal genes for COVID-19 severity, namely, *XCR1*, *CCR2*, and *SACM1L* on chromosome 3; *OAS3* on chromosome 12; *NSF* and *WNT3* on chromosome 17, *NAPSA* on chromosome 19; and *IFNAR2* on chromosome 21. Our multistage study provides new information to improve our understanding of putative causal targets for SARS-CoV-2, which could be useful for further drug repurposing efforts. The identification of additional therapeutic strategies holds the promise of reducing the public health burden of COVID-19.

Literature supports potential functional roles of several of the identified genes. *XCR1*, *CCR2*, and *SACM1L* locate at locus 3p21.31. *XCR1* is thought to mediate chemokine signaling pathways for inflammatory regulation, leukocyte chemotaxis, as well as immunopathies inducing lung injury [28]. Previous work suggested that this gene was critical for the advancement of influenza virus infection [29]. *CCR2* is known to promote chemotaxis of monocyte/macrophage towards inflammation sites [30]. It has been reported that the canonical ligand for CCR2 is highly expressed in bronchoalveolar lavage fluid from lung tissue of COVID-19 patients during mechanical ventilation [31], and circulating MCP1 levels are related to more severe disease [32]. Another study reported that *SACM1L* expression was significantly changed in response to top candidate drugs from L1000 and SARS-CoV-2 settings [33]. Furthermore, the genetic locus harboring rs17713054 was identified to be coaccessible with the promoter region of several genes including *SACM1L* in lung single cells [34]. In the earlier GWAS of the Severe Covid-19 GWAS Group, rs11385942 at this locus showed a significant association with COVID-19 severity at the genome-wide level ($P < 5\times10^{-8}$) [35]. Our work suggested that *XCR1*, *CCR2*, and *SACM1L* could potentially be the causal genes at this locus. A more recent GWAS of critical illness in COVID-19 reported a novel variant rs10735079 at chr12q24.13 in a gene cluster encoding antiviral restriction enzyme activators including *OAS3* [30]. In another study, it was also identified that a Neandertal haplotype that is protective

Table 1. Seventy-six significant gene–COVID-19 severity associations based on cross-methylome omnibus (CMO) analyses of the COVID-19 Host Genetics Initiative data (version 5; B2 outcome focusing on Europeans).

Chr	Gene	Start (build37)	End (build37)	Number of enhancer	Number of CpGs in enhancers	Number of CpGs in gene body regions	CMO *P* value[a]	False discovery rate (FDR)	Known function of the gene[b]
1	*APITD1*	10490159	10512210	0	0	11	6.58×10^{-16}	6.65×10^{-13}	Expressed at very low levels in neuroblastoma tumors; may have a role in a cell death pathway
1	*TPM3*	154127784	154167124	3	10	16	7.52×10^{-6}	3.80×10^{-3}	Variants result in autosomal dominant nemaline myopathy and other muscle disorders
2	*PLCD4*	219472488	219501907	4	11	2	4.58×10^{-11}	3.03×10^{-8}	Expression may be a marker for cancer
3	*SACM1L*	45730548	45786916	9	19	2	1.90×10^{-9}	1.21×10^{-6}	Deletion in mouse results in preimplantation lethality; involved in the organization of Golgi membranes and mitotic spindles
3	*SLC6A20*	45796942	45838027	1	4	4	4.86×10^{-29}	7.59×10^{-26}	Functions as a proline transporter expressed in kidney and small intestine; variants are associated with hyperglycinuria and iminoglycinuria
3	*LZTFL1*	45864808	45957534	2	4	10	1.22×10^{-29}	3.00×10^{-26}	Nonsense variants cause a form of Bardet–Biedl syndrome; may also function as a tumor suppressor
3	*CCR9*	45927996	45944667	1	3	4	1.82×10^{-29}	3.91×10^{-26}	A role in directing immune responses to different segments of the gastrointestinal tract; overexpressed in a variety of malignant tumors and is closely associated with tumor proliferation, apoptosis, invasion, migration and drug resistance
3	*FYCO1*	45959396	46037316	8	24	11	2.13×10^{-30}	6.37×10^{-27}	Variants are associated with inclusion body myositis and autosomal recessive congenital cataracts
3	*CXCR6*	45982425	45989845	6	16	4	2.22×10^{-30}	6.37×10^{-27}	Controls the localization of resident memory T lymphocytes to different compartments of the lung and maintains airway resident memory T lymphocytes, which are an important first line of defense against respiratory pathogens
3	*XCR1*	46058516	46069234	3	11	4	8.59×10^{-32}	1.48×10^{-27}	It transduces a signal by increasing the intracellular calcium ions level; the viral macrophage inflammatory protein II is an antagonist of this receptor and blocks signaling
3	*NRBF2P2*	46064788	46065648	0	0	2	3.19×10^{-31}	2.00×10^{-27}	A pseudogene
3	*CCR3*	46205096	46308197	0	0	11	3.48×10^{-31}	2.00×10^{-27}	May contribute to the accumulation and activation of eosinophils and other inflammatory cells in the allergic airway; also known to be an entry coreceptor for HIV-1
3	*CCR1*	46243200	46249887	5	14	4	1.10×10^{-30}	4.74×10^{-27}	Plays a role in host protection from inflammatory response, and susceptibility to virus and parasite
3	*CCR2*	46395225	46402419	4	11	5	1.24×10^{-28}	1.77×10^{-25}	Encodes a protein which is a receptor for monocyte chemoattractant protein-1, which is involved in monocyte infiltration in inflammatory diseases; protein can be a coreceptor with CD4 for HIV-1 infection
3	*CCR5*	46411633	46417697	2	4	2	4.63×10^{-29}	7.59×10^{-26}	This protein is expressed by T cells and macrophages, and is known to be an important coreceptor for macrophage-tropic virus, including HIV, to enter host cells

Table 1 continued

Chr	Gene	Start (build37)	End (build37)	Number of enhancer	Number of CpGs in enhancers	Number of CpGs in gene body regions	CMO *P* value[a]	False discovery rate (FDR)	Known function of the gene[b]
3	*CCRL2*	46448654	46454488	6	15	4	4.31×10^{-29}	7.59×10^{-26}	Expressed at high levels in primary neutrophils and primary monocytes, and is further upregulated on neutrophil activation and during monocyte to macrophage differentiation
3	*RTP3*	46538981	46542439	4	16	4	1.27×10^{-12}	1.09×10^{-9}	Related pathways include signaling by GPCR and olfactory transduction
5	*FTH1P10*	17353804	17354733	0	0	2	3.17×10^{-5}	0.01	A pseudogene
5	*SLC30A5*	68389473	68426896	4	10	2	1.15×10^{-25}	1.41×10^{-22}	Encodes a member of the SLC30A/ZnT family of zinc transporter proteins; ZnT proteins mediate both cellular zinc efflux and zinc sequestration into membrane-bound organelles
5	*MARVELD2*	68710939	68740157	2	14	8	2.10×10^{-25}	2.41×10^{-22}	Encoded protein helps establish epithelial barriers such as those in the organ of Corti, where these barriers are required for normal hearing; defects in this gene are a cause of deafness autosomal recessive type 49
5	*OCLN*	68788119	68853931	1	6	6	5.73×10^{-26}	7.58×10^{-23}	Variants in this gene are thought to be a cause of band-like calcification with simplified gyration and polymicrogyria (BLC-PMG), an autosomal recessive neurologic disorder that is also known as pseudo-TORCH syndrome
5	*RAPGEF6*	130759614	130970929	2	3	4	2.19×10^{-4}	0.05	Associated with schizoid personality disorder
6	*SPDEF*	34505579	34524110	1	6	7	1.19×10^{-4}	0.03	Highly expressed in the prostate epithelial cells, and functions as an androgen-independent transactivator of prostate-specific antigen (PSA) promoter; higher expression of this protein has also been reported in brain, breast, lung, and ovarian tumors, compared to the corresponding normal tissues
7	*SVOPL*	138279030	138386097	1	2	6	2.02×10^{-5}	9.38×10^{-3}	The protein encoded by this gene is thought to be a member of solute carrier family 22, which includes transmembrane proteins that transport toxins and drugs from the body
9	*DDX31*	135468384	135545788	6	19	2	9.78×10^{-5}	0.03	Putative RNA helicase likely implicated in a number of cellular processes involving alteration of RNA secondary structure such as translation initiation, nuclear and mitochondrial splicing, and ribosome and spliceosome assembly
9	*GTF3C4*	135545422	135570342	4	18	1	9.22×10^{-5}	0.02	Essential for RNA polymerase III to make a number of small nuclear and cytoplasmic RNAs, including 5S RNA, tRNA, and adenovirus-associated (VA) RNA of both cellular and viral origin
9	*RALGDS*	135973107	136039301	2	13	20	4.57×10^{-5}	0.02	Associated with dystonia 16 and cardiofaciocutaneous syndrome 1
9	*GBGT1*	136028340	136039332	2	17	6	2.91×10^{-5}	0.01	Encodes a glycosyltransferase that plays a role in the synthesis of Forssman glycolipid (FG); glycolipids such as FG form attachment sites for the binding of pathogens to

Table 1 continued

Chr	Gene	Start (build37)	End (build37)	Number of enhancer	Number of CpGs in enhancers	Number of CpGs in gene body regions	CMO *P* value[a]	False discovery rate (FDR)	Known function of the gene[b]
									cells; expression of this protein may determine host tropism to microorganisms; associated with inflammatory bowel disease 19 and Niemann–Pick disease, type C1
9	*OBP2B*	136080664	136084630	1	2	1	3.32×10^{-6}	1.78×10^{-3}	Probably binds and transports small hydrophobic volatile molecules
9	*LCN1P1*	136100292	136103993	0	0	1	7.09×10^{-6}	3.69×10^{-3}	A pseudogene, may bind a variety of ligands including lipids
9	*SURF1*	136218610	136223552	0	0	3	5.42×10^{-5}	0.02	Defects are a cause of Leigh syndrome, a severe neurological disorder that is commonly associated with systemic cytochrome c oxidase deficiency
9	*SURF2*	136223428	136228045	0	0	2	2.16×10^{-4}	0.05	Associated with hypotonia–cystinuria syndrome
9	*SURF4*	136228325	136242970	0	0	4	1.33×10^{-5}	6.37×10^{-3}	Associated with colorectal cancer, hereditary nonpolyposis, type 2 and macular degeneration, age-related, 6
9	*C9orf96*	136243117	136271220	0	0	2	4.51×10^{-5}	0.02	Annotates to transferase activity, transferring phosphorus-containing groups and protein tyrosine kinase activity
9	*SLC2A6*	136336217	136344259	2	13	5	2.33×10^{-5}	0.01	Probable sugar transporter that acts as a regulator of glycolysis in macrophages; associated with endometrial clear cell adenocarcinoma and testis seminoma
9	*TMEM8C*	136379708	136393734	0	0	2	4.80×10^{-5}	0.02	Involved in skeletal muscle regeneration in response to injury by mediating the fusion of satellite cells with injured myofibers; also involved in skeletal muscle hypertrophy
9	*BRD3*	136895427	136933657	6	21	6	1.29×10^{-4}	0.03	Chromatin reader that recognizes and binds hyperacetylated chromatin and plays a role in the regulation of transcription; regulates transcription by promoting the binding of the transcription factor GATA1 to its targets; associated with foodborne botulism and wound botulism
10	*NCOA4*	51565108	51590734	0	0	1	6.40×10^{-21}	6.87×10^{-18}	Enhances the androgen receptor transcriptional activity in prostate cancer cells; associated with differentiated thyroid carcinoma and withdrawal disorder
10	*RHOBTB1*	62629196	62761198	3	7	11	1.78×10^{-4}	0.04	Associated with ascaridiasis and deafness, autosomal recessive 104
12	*OAS3*	113376157	113411054	2	4	4	2.76×10^{-8}	1.63×10^{-5}	Plays a significant role in the inhibition of cellular protein synthesis and viral infection resistance
12	*OAS2*	113416200	113449528	1	1	2	2.04×10^{-6}	1.13×10^{-3}	Plays a critical role in cellular innate antiviral response
12	*DTX1*	113494514	113535833	2	4	18	9.86×10^{-6}	4.84×10^{-3}	Involved in neurogenesis, lymphogenesis and myogenesis, and may also be involved in marginal zone B (MZB) cell differentiation.

Table 1 continued

Chr	Gene	Start (build37)	End (build37)	Number of enhancer	Number of CpGs in enhancers	Number of CpGs in gene body regions	CMO *P* value[a]	False discovery rate (FDR)	Known function of the gene[b]
12	*CCDC42B*	113587663	113597081	0	0	5	7.50×10^{-7}	4.30×10^{-4}	Associated with phosphoglycerate kinase 1 deficiency and Cornelia de Lange syndrome 4 with or without midline brain defects
12	*SDSL*	113860042	113876081	4	5	2	3.03×10^{-5}	0.01	Has low serine dehydratase and threonine dehydratase activity; associated with subdural empyema and sarcocystosis
13	*TSC22D1*	45007655	45151283	5	6	3	1.82×10^{-8}	1.12×10^{-5}	The encoded protein may play a critical role in tumor suppression
17	*NSF*	44668035	44834830	0	0	2	8.06×10^{-5}	0.02	Associated with tetanus and type 1 diabetes mellitus 13
17	*WNT3*	44839872	44910520	3	10	14	2.90×10^{-5}	0.01	May play a key role in some cases of human breast, rectal, lung, and gastric cancer
19	*ZNF266*	9523272	9546254	18	67	4	8.63×10^{-5}	0.02	May be involved in transcriptional regulation
19	*ZNF121*	9671029	9695209	16	65	2	8.20×10^{-5}	0.02	May be involved in transcriptional regulation
19	*ZNF561*	9715356	9732075	19	70	1	6.86×10^{-5}	0.02	Related to pathways of gene expression and herpes simplex virus 1 infection
19	*ZNF846*	9862669	9903856	11	37	1	7.19×10^{-5}	0.02	Associated with monkeypox; related to pathways of herpes simplex virus 1 infection
19	*FBXL12*	9920943	9938492	22	77	1	7.54×10^{-5}	0.02	Mediates the polyubiquitination and proteasomal degradation of CAMK1 leading to disruption of cyclin D1/CDK4 complex assembly which results in G1 cell cycle arrest in lung epithelia; related to pathways of innate immune system and class I MHC mediated antigen processing and presentation
19	*PPAN*	10216965	10225414	23	78	11	8.34×10^{-5}	0.02	May have a role in cell growth; associated with narcolepsy
19	*EIF3G*	10225693	10230596	16	63	4	7.18×10^{-5}	0.02	Associated with narcolepsy
19	*DNMT1*	10244021	10341962	17	46	8	9.42×10^{-5}	0.02	Variation is associated with cerebellar ataxia, deafness, and narcolepsy, and neuropathy, hereditary sensory, type IE
19	*S1PR2*	10334520	10341948	3	17	1	6.32×10^{-5}	0.02	Defects have been associated with congenital profound deafness
19	*ICAM1*	10381511	10397291	4	13	8	5.63×10^{-5}	0.02	Encodes a cell surface glycoprotein which is typically expressed on endothelial cells and cells of the immune system; binds to integrins of type CD11a/CD18, or CD11b/CD18 and is also exploited by rhinovirus as a receptor; associated with malaria and hepatocellular carcinoma
19	*ICAM4*	10397643	10399198	3	16	7	4.75×10^{-5}	0.02	Associated with blood group system, Landsteiner–Wiener and anemia, congenital dyserythropoietic, type Iv; related to pathways of innate immune system and actin dynamics signaling pathway
19	*ICAM5*	10400657	10407454	3	16	12	5.93×10^{-5}	0.02	May be a critical component in neuron–microglial cell interactions in the course of normal development or as part of neurodegenerative diseases; associated with acute

Table 1 continued

Chr	Gene	Start (build37)	End (build37)	Number of enhancer	Number of CpGs in enhancers	Number of CpGs in gene body regions	CMO *P* value[a]	False discovery rate (FDR)	Known function of the gene[b]
									hemorrhagic conjunctivitis and holoprosencephaly; related to pathways of innate immune system and degradation of the extracellular matrix
19	*ZGLP1*	10415479	10420556	1	2	2	3.76×10^{-5}	0.02	Associated with hermaphroditism
19	*FDX1L*	10416103	10426691	0	0	5	9.96×10^{-5}	0.03	Associated with mitochondrial myopathy, episodic, with or without optic atrophy and reversible leukoencephalopathy and mitochondrial myopathy; related to pathways of HIV life cycle and diseases of metabolism
19	*ICAM3*	10444452	10450499	2	6	7	5.45×10^{-5}	0.02	May be the most important ligand for LFA-1 in the initiation of the immune response; contributes to apoptotic neutrophil phagocytosis by macrophages
19	*PDE4A*	10527449	10580305	4	17	21	5.93×10^{-5}	0.02	Associated with asthma and pulmonary eosinophilia
19	*CDKN2D*	10677138	10679735	6	22	3	6.12×10^{-5}	0.02	The negative regulation of the cell cycle involved in this protein was shown to participate in repressing neuronal proliferation, as well as spermatogenesis; associated with adult central nervous system primitive neuroectodermal neoplasm and parathyroid adenoma; related to pathways of immune response IL-23 signaling pathway and mitotic G1-G1/S phases
19	*AP1M2*	10683347	10697991	2	8	12	1.86×10^{-4}	0.04	Associated with Pettigrew syndrome and chromophobe renal cell carcinoma; related to pathways of vesicle-mediated transport and HIV life cycle
19	*SLC44A2*	10713133	10755235	7	27	16	2.06×10^{-4}	0.05	Associated with femoral vein thrombophlebitis and deafness, autosomal recessive 68; related to pathways of transport of glucose and other sugars, bile salts and organic acids, metal ions and amine compounds and innate immune system
19	*C19orf38*	10947251	10980466	4	15	3	7.72×10^{-5}	0.02	Unknown
19	*DOCK6*	11309971	11373157	4	20	17	8.02×10^{-5}	0.02	Associated with Adams–Oliver syndrome 2 and Adams–Oliver syndrome
19	*NAPSA*	50861734	50869087	0	0	8	1.60×10^{-4}	0.04	The encoded protease may play a role in the proteolytic processing of pulmonary surfactant protein B in the lung and may function in protein catabolism in the renal proximal tubules
21	*OLIG2*	34398153	34401504	3	5	16	3.83×10^{-12}	2.86×10^{-9}	Required for oligodendrocyte and motor neuron specification in the spinal cord, as well as for the development of somatic motor neurons in the hindbrain
21	*OLIG1*	34442450	34444726	0	0	10	2.78×10^{-12}	2.27×10^{-9}	Associated with oligodendroglioma and anaplastic astrocytoma; related to pathways of neural crest differentiation and neural stem cell differentiation pathways and lineage-specific markers
21	*IFNAR2*	34602206	34637980	5	17	7	3.89×10^{-15}	3.52×10^{-12}	Associated with immunodeficiency 45 and primary immunodeficiency with post–measles–mumps–rubella

Table 1 continued

Chr	Gene	Start (build37)	End (build37)	Number of enhancer	Number of CpGs in enhancers	Number of CpGs in gene body regions	CMO *P* value[a]	False discovery rate (FDR)	Known function of the gene[b]
									vaccine viral infection; related to pathways of measles and innate immune system
21	*IL10RB*	34638663	34669539	2	6	2	2.59×10^{-15}	2.47×10^{-12}	Associated with inflammatory bowel disease 25, autosomal recessive and hepatitis B; related to pathways of immune response IL-23 signaling pathway and innate immune system
21	*IFNAR1*	34696734	34732168	1	2	3	2.98×10^{-12}	2.32×10^{-9}	Functions as an antiviral factor; associated with hepatitis C and yellow fever; related to pathways of measles and innate immune system
21	*IFNGR2*	34775202	34851655	1	9	7	1.29×10^{-11}	9.21×10^{-9}	Associated with immunodeficiency 28 and autosomal dominant Mendelian susceptibility to mycobacterial diseases due to partial IFNgammaR2 deficiency; related to pathways of innate immune system and PEDF induced signaling
21	*DNAJC28*	34860497	34864027	2	10	1	1.77×10^{-11}	1.22×10^{-8}	Associated with Mullegama–Klein–Martinez syndrome and microphthalmia, syndromic 10

[a]*P* value derived from association analyses of 9,986 hospitalized patients and 1,877,672 population controls (two-sided); associations with FDR ≤ 0.05 were shown.
[b]Based on search of GeneCards on 25 April 2021.

Table 2. Significant predicted gene expression in blood–COVID-19 associations for the cross-methylome omnibus (CMO) identified genes based on the COVID-19 Host Genetics Initiative data.

Chr	Gene[a]	R^{2b}	Number of predicting SNPs	Hospitalized patients versus population controls				Very severe respiratory confirmed COVID versus controls	
				OR (95% CI)[c]	*P* value[d]	FDR *P* value[d]	FOGS *P* value	OR (95% CI)[c]	*P* value[e]
3	***XCR1***	0.04	40	2.49 (1.72–3.60)	1.51×10^{-6}	3.61×10^{-5}	1.00×10^{-7}	4.59 (2.54–8.29)	4.68×10^{-7}
3	***CCR2***	0.05	4	2.68 (1.35–5.34)	0.005	0.03	0.006	5.06 (1.68–15.23)	3.89×10^{-3}
3	*CCR5*	0.05	46	0.51 (0.32–0.82)	0.006	0.03	-	0.95 (0.71–1.29)	0.76
3	***SACM1L***	0.06	49	0.69 (0.53–0.91)	0.009	0.04	1.00×10^{-7}	0.68 (0.46–1.01)	0.06
12	***OAS3***	0.02	37	2.15 (1.57–2.94)	2.00×10^{-6}	3.61×10^{-5}	1.00×10^{-7}	3.61 (2.24–5.81)	1.32×10^{-7}
17	***NSF***	0.02	65	0.45 (0.30–0.68)	1.70×10^{-4}	2.04×10^{-3}	1.00×10^{-7}	0.60 (0.34–1.06)	0.08
17	***WNT3***	0.02	19	0.56 (0.40–0.79)	9.52×10^{-4}	6.85×10^{-3}	1.00×10^{-7}	0.57 (0.33–1.00)	0.05
19	***NAPSA***	0.04	5	0.46 (0.30–0.71)	5.18×10^{-4}	4.66×10^{-3}	0.002	0.29 (0.15–0.57)	2.56×10^{-4}
21	***IFNAR2***	0.06	134	0.79 (0.67–0.92)	0.004	0.02	0.003	0.71 (0.57–0.88)	2.09×10^{-3}

FDR false discovery rate, *FOGS* fine-mapping of gene sets, *SNP* single-nucleotide polymorphism.
[a]Bolded genes are putatively causal genes.
[b]R^2: model prediction performance (R^2).
[c]Odds ratio (OR) and confidence interval (CI) per one standard deviation increase in genetically predicted gene expression.
[d]*P* value derived from association analyses of 9,986 hospitalized patients and 1,877,672 population controls (two-sided); associations with FDR ≤ 0.05 were shown.
[e]*P* value derived from association analyses of 5,101 very severe respiratory confirmed COVID patients and 1,383,241 population controls (two-sided).

Table 3. Predicted gene expression in lung–COVID-19 associations for the putative causal genes based on the COVID-19 Host Genetics Initiative data.

Chr	Gene	R^{2a}	Number of predicting snps	Hospitalized patients versus population controls		Very severe respiratory confirmed COVID versus controls	
				OR (95% CI)[b]	*P* value[c]	OR (95% CI)[b]	*P* value[d]
3	*CCR2*	0.01	4	2.81 (1.37–5.76)	4.71×10^{-3}	5.50 (1.75–17.25)	3.49×10^{-3}
17	*WNT3*	0.16	19	0.79 (0.70–0.90)	4.85×10^{-4}	0.81 (0.66–0.98)	0.03
21	*IFNAR2*	0.10	127	0.74 (0.65–0.84)	3.01×10^{-6}	0.84 (0.70–1.00)	0.05

[a]R^2: model prediction performance (R^2).
[b]Odds ratio (OR) and confidence interval (CI) per one standard deviation increase in genetically predicted gene expression.
[c]*P* value derived from association analyses of 9,986 hospitalized patients and 1,877,672 population controls (two-sided).
[d]*P* value derived from association analyses of 5,101 very severe respiratory confirmed COVID patients and 1,383,241 population controls (two-sided).

against severe COVID-19 contains all or parts of three genes including *OAS3*. Interestingly, the SNPs showing the most significant associations are in *OAS3* [36]. *IFNAR2* at chromosome 21 encodes type I interferon (IFN-α/β), which is known to play a key role in human antiviral immunity [37]. Previous work reported that probes tagging this gene showed pleiotropic association with hospitalized COVID-19 [38]. Some of the genes suggested by CMO test but not following S-PrediXcan analyses may also warrant further investigation. For 42 of the genes, their genetic expression prediction models were not established using the modified UTMOST modeling strategy. For the S-PrediXcan analyses, the odd ratios reported in this study were for genetically predicted expression but not actual expression levels. Further functional validation to better understand the exact roles of these genes is needed.

A previous study reported likely causal links of *IFNAR2*, *TYK2*, and *CCR2* with COVID-19 critical illness [30]. In the current study, we also identified *IFNAR2* and *CCR2*. In another study analyzing an earlier version of COVID-19 HGI data (version 4), genes *IFNAR2* and *CCR2* were identified with allelic imbalance evidence at COVID-19 GWAS risk variants (unpublished data). *IFNAR2* was also associated with migraine and throat pain (unpublished data). The genetically predicted expression of *IFNAR2* was further identified to be inversely associated with creatine kinase. In this study, *XCR1* and *OAS3* were also implicated as likely susceptibility genes for COVID-19 severity, which was consistent with our findings. In the COVID-19 HGI main manuscript (unpublished data), it was identified that the COVID-19 associated variants modified the expression of *OAS1*/*OAS3*/*OAS2* (12q24.13) and *IFNAR2*/*IL10RB* (21q22.11) in lung. Overall, besides identifying literature reported genes, in this work we also identified several novel putative causal genes for COVID-19.

There are several potential limitations in our study. First, due to the nature of COVID-19 HGI, it is possible that although all are required to meet the phenotype definition (e.g., be hospitalized COVID-19 patients), the included cases in different substudies are not completely homogeneous. For example, the criteria for COVID-19 patients' hospitalization could be different across studies/regions, thus measurement errors could exist. Second, in our analyses, we were not able to comprehensively adjust for underlying cardiovascular and metabolic factors that are reported to be related to COVID-19 [39]. While a majority of implicated genes (except for *OAS3* [40]) have not been reported to be associated with cardiovascular and metabolic factors according to GWAS Catalog, alleviating the concern of pleiotropy, further work with adjustment of such variables is needed to validate our findings. Third, in the data sets used in our analyses, information about the infection status of SARS-CoV-2 in the control participants was limited. By using the general population as controls, severe COVID-19 cases are actually compared with a large cohort of individuals who may or may not develop severe COVID-19 upon exposure to the virus. However, the presence of susceptible subjects in the control group, if any, is expected to only bias the results toward the null. Future work using cleaner controls would be necessary to better characterize the relationship. Fourth, the current study focuses on Europeans, the ethnic group with the largest available sample size. It would be critical to conduct analyses focusing on other ethnic groups, to enhance the generalizability of findings of such work. Currently, the available sample size of GWAS of COVID-19 in non-European populations is relatively small. For example, in the COVID HGI, for the B2 outcome, data are available for only 257 cases of Latinos, 60 cases of Arabs, 948 of Admixed Americans, 790 of Africans, 186 of South Asians, and 1,414 of East Asians. The power for such analyses would be relatively low. Additional work for sex specific analyses would be needed as well. We currently do not have the data available for sex specific analyses. Finally, besides the outcomes evaluated in the current study, analyses using brain tissue gene expression models could be helpful for characterizing factors related to the neurological symptoms of COVID-19. The available data in the COVID HGI may not be appropriate for testing this, as neurological symptoms may manifest in mildly symptomatic COVID-19 individuals. Future work leveraging cleaner disease phenotype is needed for testing this.

In conclusion, in a large scale multiphase integrative multiomics study with complementary methods, we identified eight putative causal genes at five loci for COVID-19 severity. Such findings will be very meaningful for guiding future drug repurposing efforts aiming to reduce the COVID-19 public health burden.

DATA AVAILABILITY

All data and methods used in the analysis are described or included in this article and the electronic supplementary information. The COVID-19 HGI GWAS summary statistics are deposited at http://www.covid19hg.org/results/r5/. The blood methylation prediction models are available at http://bbmri.researchlumc.nl/atlas/#data. The data for running the CMO test are available at http://www.zenodo.org/record/4475935#.YItjZi2cY0w. The blood and lung tissue gene expression prediction models are available at http://www.zenodo.org/record/3842289#.YHqHcehKiUk.

CODE AVAILABILITY

Access to the custom code may be requested from the corresponding authors.

Received: 28 March 2021; Revised: 24 May 2021; Accepted: 27 May 2021;
Published online: 28 June 2021

REFERENCES

1. Hoffmann M, Kleine-Weber H, Schroeder S, Krüger N, Herrler T, Erichsen S, et al. SARS-CoV-2 cell entry depends on ACE2 and TMPRSS2 and is blocked by a clinically proven protease inhibitor. Cell. 2020;181:271–80.e8.

2. Richardson S, Hirsch JS, Narasimhan M, Crawford JM, McGinn T, Davidson KW et al. Presenting characteristics, comorbidities, and outcomes among 5700 patients hospitalized with COVID-19 in the New York city area. JAMA. 2020;323:2052–9.
3. Wu C, Pan W. Integration of methylation QTL and enhancer-target gene maps with schizophrenia GWAS summary results identifies novel genes. Bioinformatics. 2019;35:3576–83.
4. Hu Y, Li M, Lu Q, Weng H, Wang J, Zekavat SM, et al. A statistical framework for cross-tissue transcriptome-wide association analysis. Nat Genet. 2019;51:568–76.
5. Wu C, Pan W. Integrating eQTL data with GWAS summary statistics in pathway-based analysis with application to schizophrenia. Genet Epidemiol. 2018;42:303–16.
6. Gusev A, Ko A, Shi H, Bhatia G, Chung W, Penninx BW, et al. Integrative approaches for large-scale transcriptome-wide association studies. Nat Genet. 2016;48:245–52.
7. Gamazon ER, Wheeler HE, Shah KP, Mozaffari SV, Aquino-Michaels K, Carroll RJ, et al. A gene-based association method for mapping traits using reference transcriptome data. Nat Genet. 2015;47:1091–8.
8. Wu L, Wang J, Cai Q, Cavazos TB, Emami NC, Long J, et al. Identification of novel susceptibility loci and genes for prostate cancer risk: A Transcriptome-wide Association Study in over 140,000 European descendants. Cancer Res. 2019;79:3192–204.
9. Wu C, Pan W. Integration of enhancer-promoter interactions with GWAS summary results identifies novel Schizophrenia-associated genes and pathways. Genetics. 2018;209:699–709.
10. Wu L, Shi W, Long J, Guo X, Michailidou K, Beesley J, et al. A transcriptome-wide association study of 229,000 women identifies new candidate susceptibility genes for breast cancer. Nat Genet. 2018;50:968–78.
11. Zhong J, Jermusyk A, Wu L, Hoskins JW, Collins I, Mocci E, et al. A Transcriptome-Wide Association Study (TWAS) identifies novel candidate susceptibility genes for pancreatic cancer. J Natl Cancer Inst. 2020;112:1003–12.
12. Yang Y, Wu L, Shu XO, Cai Q, Shu X, Li B, et al. Genetically predicted levels of DNA methylation biomarkers and breast cancer risk: data from 228 951 women of European descent. J Natl Cancer Inst. 2020;112:295–304.
13. Yang Y, Wu L, Shu X, Lu Y, Shu XO, Cai Q, et al. Genetic data from nearly 63,000 women of European descent predicts DNA methylation biomarkers and epithelial ovarian cancer risk. Cancer Res. 2019;79:505–17.
14. Furlong EEM, Levine M. Developmental enhancers and chromosome topology. Science. 2018;361:1341–5.
15. Wu C, Bradley J, Li Y, Wu L, Deng HW. A gene-level methylome-wide association analysis identifies novel Alzheimer's disease genes. Bioinformatics 2021. https://doi.org/10.1093/bioinformatics/btab045.
16. Wainberg M, Sinnott-Armstrong N, Mancuso N, Barbeira AN, Knowles DA, Golan D, et al. Opportunities and challenges for transcriptome-wide association studies. Nat Genet. 2019;51:592–9.
17. Mancuso N, Freund MK, Johnson R, Shi H, Kichaev G, Gusev A, et al. Probabilistic fine-mapping of transcriptome-wide association studies. Nat Genet. 2019;51:675–82.
18. Barfield R, Feng H, Gusev A, Wu L, Zheng W, Pasaniuc B, et al. Transcriptome-wide association studies accounting for colocalization using Egger regression. Genet Epidemiol. 2018;42:418–33.
19. Wu C, Pan W. A powerful fine-mapping method for transcriptome-wide association studies. Hum Genet. 2020;139:199–213.
20. COVID-19 Host Genetics Initiative. The COVID-19 Host Genetics Initiative, a global initiative to elucidate the role of host genetic factors in susceptibility and severity of the SARS-CoV-2 virus pandemic. Eur J Hum Genet 2020;28:715–8.
21. Fishilevich S, Nudel R, Rappaport N, Hadar R, Plaschkes I, Stein TI, et al. GeneHancer: genome-wide integration of enhancers and target genes in GeneCards. Database 2017;2017:bax028.
22. Baselmans BML, Jansen R, Ip HF, van Dongen J, Abdellaoui A, van de Weijer MP, et al. Multivariate genome-wide analyses of the well-being spectrum. Nat Genet. 2019;51:445–51.
23. Liu YXJ. Cauchy combination test: a powerful test with analytic p-value calculation under arbitrary dependency structures. J Am Stat Assoc. 2020;115:393–402.
24. Barbeira AN, Dickinson SP, Bonazzola R, Zheng J, Wheeler HE, Torres JM, et al. Exploring the phenotypic consequences of tissue specific gene expression variation inferred from GWAS summary statistics. Nat Commun. 2018;9:1825.
25. Consortium GT. The GTEx Consortium atlas of genetic regulatory effects across human tissues. Science. 2020;369:1318–30.
26. Liu D, Zhou D, Sun Y, Zhu J, Ghoneim D, Wu C, et al. A Transcriptome-Wide Association Study identifies candidate susceptibility genes for pancreatic cancer risk. Cancer Res. 2020;80:4346–54.
27. Zhou D, Jiang Y, Zhong X, Cox NJ, Liu C, Gamazon ER. A unified framework for joint-tissue transcriptome-wide association and Mendelian randomization analysis. Nat Genet. 2020;52:1239–46.
28. McCoy K, Peterson A, Tian Y, Sang Y. Immunogenetic Association underlying severe COVID-19. Vaccines. 2020;8:700.
29. Vastrad B, Vastrad C, Tengli A. Identification of potential mRNA panels for severe acute respiratory syndrome coronavirus 2 (COVID-19) diagnosis and treatment using microarray dataset and bioinformatics methods. 3 Biotech. 2020;10:422.
30. Pairo-Castineira E, Clohisey S, Klaric L, Bretherick AD, Rawlik K, Pasko D, et al. Genetic mechanisms of critical illness in Covid-19. Nature. 2021; 591:92–8.
31. Zhou Z, Ren L, Zhang L, Zhong J, Xiao Y, Jia Z, et al. Heightened innate immune responses in the respiratory tract of COVID-19 patients. Cell Host Microbe. 2020;27:883–90.e2.
32. Zhao Y, Qin L, Zhang P, Li K, Liang L, Sun J, et al. Longitudinal COVID-19 profiling associates IL-1RA and IL-10 with disease severity and RANTES with mild disease. JCI Insight. 2020;5:e139834.
33. El-Hachem N, Eid E, Nemer G, Dbaibo G, Abbas O, Rubeiz N, et al. Integrative transcriptome analyses empower the anti-COVID-19 drug arsenal. iScience. 2020;23:101697.
34. Wang A, Chiou J, Poirion OB, Buchanan J, Valdez MJ, Verheyden JM, et al. Single-cell multiomic profiling of human lungs reveals cell-type-specific and age-dynamic control of SARS-CoV2 host genes. Elife. 2020;9:e62522.
35. Severe Covid-19 GWAS Group, Ellinghaus D, Degenhardt F, Bujanda L, Buti M, Albillos A, et al. Genomewide Association Study of Severe Covid-19 with respiratory failure. N Engl J Med. 2020;383:1522–34.
36. Zeberg H, Paabo S. A genomic region associated with protection against severe COVID-19 is inherited from Neandertals. Proc Natl Acad Sci USA 2021;118:e20263091.
37. Duncan CJ, Mohamad SM, Young DF, Skelton AJ, Leahy TR, Munday DC, et al. Human IFNAR2 deficiency: lessons for antiviral immunity. Sci Transl Med. 2015;7:307ra154.
38. Liu D, Yang J, Feng B, Lu W, Zhao C, Li L. Mendelian randomization analysis identified genes pleiotropically associated with the risk and prognosis of COVID-19. J Infect. 2021;82:126–32.
39. Williamson EJ, Walker AJ, Bhaskaran K, Bacon S, Bates C, Morton CE, et al. OpenSAFELY: factors associated with COVID-19 death in 17 million patients. Nature 2020; 10.1038/s41586-020-2521-4.
40. Liu M, Jin HS, Park S. Protein and fat intake interacts with the haplotype of PTPN11_rs11066325, RPH3A_rs886477, and OAS3_rs2072134 to modulate serum HDL concentrations in middle-aged people. Clin Nutr. 2020;39:942–9.

ACKNOWLEDGEMENTS

We would like to acknowledge COVID-19 Host Genetics Initiative for making their COVID-19 GWAS summary statistics to be available.

FUNDING

This research is supported by University of Hawaii Cancer Center and Florida State University. D.L. is partially supported by the Harbin Medical University Cancer Hospital. Y.S. is partially supported by the Department of Education of Fujian Province, P. R. China.

COMPETING INTERESTS

The authors declare no competing interests.

ETHICS DECLARATION

This study was reviewed by the University of Hawaii Institutional Review Board (2019-00402). All individuals participating in the COVID HGI study properly signed the informed consent according to the participating studies' Institutional Review Board. All data were de-identified before the analysis of the current study.

ROLE OF THE FUNDER/SPONSOR

The funding organization had no role in the design and conduct of the study; collection, management, analysis, and interpretation of the data; preparation, review, or approval of the manuscript; or decision to submit the manuscript for publication.

ADDITIONAL INFORMATION

Supplementary information The online version contains supplementary material available at https://doi.org/10.1038/s41436-021-01243-5.

Correspondence and requests for materials should be addressed to L.W. or C.W.

Reprints and permission information is available at http://www.nature.com/reprints

Publisher's note Springer Nature remains neutral with regard to jurisdictional claims in published maps and institutional affiliations.